

# Proper Orthogonal Decomposition and Bilinear Lyapunov Control of Parabolic Trough Collectors\*

Tim Reuscher<sup>1</sup>, Lorenz Pyta<sup>1</sup>, Thomas Konrad<sup>1</sup>, Pascal Richter<sup>2</sup>, Dirk Abel<sup>1</sup>

**Abstract**—To ensure economic and safe operation of parabolic trough collectors a precise control of the output temperature of the troughs is necessary. Here, promising control algorithms as the recently proposed bilinear Lyapunov controller have been formulated. Drawbacks of this controller design are a row of simplifying assumptions along with a rough system description, which results in strict limits of the controller gain, as the control loop tends to high frequent oscillation otherwise. Those problems are treated in this work by use of model reduction involving proper orthogonal decomposition and alternative formulations of the control problem, which relax some of the assumptions. In consequence, an improved version of the bilinear Lyapunov control - with robust performance and zero tracking error proven - and potentially higher controller gains is proposed. Realistic simulations confirm the theoretical results while showing shorter rise times without the risk of high frequent oscillations.

## I. INTRODUCTION

The public debate about energy consumption and climate change is dominated by the need to find clean yet effective methods of creating electrical power. Parabolic trough solar collector systems are part of a strategy for global regenerative power generation. The global trends in renewable investments report 2018 [1] shows a high interest in investment into sources of renewable energy, making the solar trough technology more and more attractive.

A parabolic trough solar collector system is composed of parallel loops of parabolic troughs. Each trough consists of a parabolic mirror which focuses incoming sunlight onto a pipe containing thermal oil, which is pumped through the pipe and used for generation of electric energy. A simplified representation of one parallel loop is displayed in Fig. 1. In order to achieve high efficiencies in electrical power generation, a high oil temperature at the outlet is desirable. However, as the oil decomposes when above a critical temperature, it cannot be heated to arbitrarily high temperatures [2]. Here, sudden changes in cloud coverage influence the solar intensity and thus create an influential disturbance onto the output temperature with high volatility. Accordingly, the incorporation of feedback control becomes necessary.

\*Funded by the Excellence Initiative of the German federal and state governments.

<sup>1</sup>Tim Reuscher, Lorenz Pyta, Thomas Konrad and Dirk Abel are with the Institute of Automatic Control, RWTH Aachen, Campus Boulevard 30 Aachen, Germany {t.reuscher, l.pyta, t.konrad, d.abel}@irt.rwth-aachen.de

<sup>2</sup>Pascal Richter is with the Research Group Theory of Hybrid Systems, RWTH Aachen University, Ahornstr. 55, Aachen, Germany pascal.richter@rwth-aachen.de

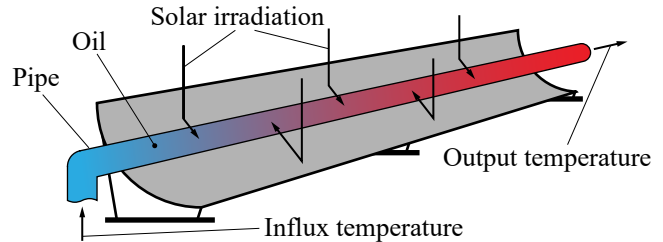


Fig. 1. Single parabolic trough taken from a solar collector system with parallel loops

An extended overview of control approaches for parabolic trough collectors can be found in [3]. The range of applied control schemes ranges from PID controllers in [4] to more advanced methods such as model predictive approaches based on linearized plant models (see, e.g., [5]) or on nonlinear models, e. g., [6]. Also approaches with explicit consideration of system nonlinearities [7] or robust control [8] can be found. Furthermore, a very promising approach based on bilinear Lyapunov control has been presented in [9] and [10] with the benefits of proving robust stability and zero tracking error. Unfortunately, the bilinear Lyapunov control only allows very small controller gains, as the description of the plant relies on several assumptions and the use of rough approximate models. Hence, despite the beneficial theoretical foundation, the bilinear Lyapunov control from [10] needs to be improved.

In this work, three improvements of the bilinear Lyapunov control are presented. First, the approximate models are improved by use of the proper orthogonal decomposition (POD) as model reduction technique. Second, the formulation of the controller in [9] and [10] is generalized such that some assumptions can be dropped. And third, a dynamic approach to parameter selection is applied. The improvements achieve possible selection of higher controller gains.

The structure of this paper is as follows: Beginning with a brief description of the plant model in Section II, the recently proposed bilinear Lyapunov control is presented in Section III. Thereafter, an improving model reduction procedure is presented in Section IV. In Section V the extensions of the bilinear Lyapunov control are presented. Simulation results for the designed controller in Section VI and the summary in VII conclude the paper.

## II. PLANT MODEL

In order to create an efficient controller for the parabolic trough solar collector, analytic modeling of the plant is necessary. The system dynamics can be split into two separate parts: The dynamic of the fluid inside the pipe and the temperature distribution of the pipe wall itself.

### A. Temperature dynamic of the fluid

For the temperature distribution along the pipe, the first law of thermodynamics is applied to an infinitesimally sized fluid particle. Convection of heat along the direction of fluid transport can be neglected due to high Peclet-numbers of the process. No temperature gradient in radial direction is considered due to the thinness of the pipe walls. Also, the fluid is assumed to be incompressible, which is a reasonable assumption for oils. The resulting equation for the temperature distribution of the oil reads

$$\frac{dT}{dt}(x, t) + u(t) \frac{dT}{dx}(x, t) = s(x, t), \quad (1)$$

where  $t \in [0, t_{\text{end}}]$  is the time,  $x \in [0, L]$  the spatial coordinate,  $T(x, t)$  the fluid temperature distribution along the pipe and  $s(x, t) = \frac{\dot{q}}{(\rho c_p A)_{\text{fluid}}}$  the disturbance due to the energy flow  $\dot{q}$  transferred from the pipe wall to the oil. The biggest errors in this equation as opposed to reality are in the heat capacity  $c_p$  and the density of the fluid  $\rho$  being considered constant with respect to temperature. Research suggests an error of below 5%. Also, the pipe diameter  $A$  is assumed to be constant. The temperature of the fluid entering at  $x = 0$  is incorporated as a left boundary condition  $T(0, t) = T_1(t)$ . Together with initial values the partial differential equation (PDE) (1) for the axial temperature reads

$$\begin{cases} \frac{dT}{dt} + u \frac{dT}{dx} = s(x, t) \\ T(0, t) = T_1(t), \quad T(x, 0) = T_0(x). \end{cases} \quad (2)$$

### B. Temperature dynamic of the wall

Applying the first law of thermodynamics equivalently to an infinitesimally sized part of the pipe wall, assuming again no axial conduction of heat and no temperature gradients in radial direction, the axial temperature distribution of the pipe wall reads as

$$\begin{cases} \frac{d\vartheta}{dt} + \widehat{\lambda}(\vartheta(x, t) - T(x, t)) = p(x, t) \\ \vartheta(x, 0) = \vartheta_0(x) \end{cases}, \quad (3)$$

where  $\vartheta(x, t)$  is the wall temperature,  $\widehat{\lambda} = \frac{\lambda}{(\rho c_p A)_{\text{pipe}}}$  describes the heat transfer between pipe wall and fluid with a heat transfer coefficient  $\lambda$  assumed to be constant. The term  $p(x, t)$  is calculated from the solar irradiance  $I(x, t)$  with the efficiency  $\nu$  of the used mirrors and the size of the optical aperture  $G$

$$p(x, t) = \frac{\nu G}{(\rho c_p A)_{\text{pipe}}} I(x, t). \quad (4)$$

### C. Full system dynamic

The dynamic of the full system including pipe wall and fluid temperatures is then given in (5)

$$\begin{cases} \frac{dT}{dt} = -u \frac{dT}{dx} + \widehat{\lambda}(\vartheta(x, t) - T(x, t)) \\ \frac{d\vartheta}{dt} = \widehat{\lambda}(T(x, t) - \vartheta(x, t)) + p(x, t) \\ T(0, t) = T_1(t), \quad T(x, 0) = T_0(x), \quad \vartheta(x, 0) = \vartheta_0(x). \end{cases} \quad (5)$$

The PDE (2) is coupled with an ordinary differential equation (3) to represent the heat transfer between wall and fluid. Losses have been neglected in this analysis, as modern coating technologies reduce the amount of radiative heat loss, while convective heat loss can be minimized by modern glass encasings [11]. This modeling approach is not new, but has so far not been used in the context of bilinear Lyapunov control.

## III. STATE OF THE ART

In [9] and [10], Elmetennani et al. introduced an approximate model method based on radial Gaussian functions for the system (2) and a bilinear Lyapunov controller using this model reduction. To properly understand the changes and extensions proposed in the present paper, the original method by Elmetennani et al. is explained. This entire section is a summary of the works of Elmetennani et al. in [9] and [10]. For further detail, refer to [9] and [10]

### A. Approximate model

The approximate model uses the separation principle

$$T(x, t) = \sum_{j=1}^{\infty} \gamma_j(x) \xi_j(t) \quad (6)$$

with spatial basis functions  $\gamma_j(x)$  and temporal weight functions  $\xi_j(t)$ . The basis functions  $\gamma_j(x)$  are fixed as radial Gaussian functions

$$\mu_j(x) = \exp\left(-\frac{1}{2} \left(\frac{x - m_j}{\sigma_j}\right)^2\right), \quad (7)$$

which are distributed along the length of the pipe with their mean value  $m_d$ . To remove bias from the basis functions  $\mu_j(x)$ , they are scaled such that  $\sum_{j=1}^d \gamma_j(x) = 1$  holds:

$$\gamma_j(x) = \frac{\mu_j(x)}{\sum_{j=1}^d \mu_j(x)}. \quad (8)$$

Equation (8) already includes the reduction of dimension. The infinite sum from (6) has been reduced to  $d$  summands, thereby reducing the system order to  $d$ . This reduction leads to the approximate temperature distribution

$$T(x, t) \approx \widehat{T}(x, t) = \sum_{j=1}^d \gamma_j(x) \xi_j(t). \quad (9)$$

Uniform spatial discretization with  $N_x$  knots with a distance  $\Delta x$  and replacing  $\widehat{T}(x, t)$  with a spatially discrete  $\widehat{T}(t) = [\widehat{T}(0, t), \dots, \widehat{T}(N_x \Delta x, t)]$  in (2) results in

$$\Gamma \dot{\xi}(t) + u \Gamma_x \xi(t) = S(t), \quad (10)$$

with  $\Gamma \in \mathbb{R}^{N_x \times d}$  being a column matrix of the values of each  $\gamma_j$  at the mentioned grid points and  $\Gamma_x$  for  $\frac{d\gamma_j}{dx}$ .  $S(t) \in \mathbb{R}^{N_x}$  is the column matrix containing the spatially discretized values of  $s(x, t)$ . Introducing  $A = -(\Gamma^T \Gamma)^{-1} \Gamma^T \Gamma_x$ ,  $B = (\Gamma^T \Gamma)^{-1} \Gamma^T S(t)$  and  $C = [\gamma_1(L), \dots, \gamma_d(L)]$  the system can be brought into nonlinear state space form

$$\begin{cases} \dot{\xi}(t) = A\xi(t)u + B(t) \\ y(t) = \hat{T}(L, t) = C\xi(t) \\ \xi(0) = (\Gamma^T \Gamma)^{-1} \Gamma^T \hat{T}(0) . \end{cases} \quad (11)$$

### B. Control structure

The controller is designed using the Lyapunov stability criterion. Thereby, the tracking problem is split into two parts:

- 1) Define a nominal plant with constant disturbance  $\bar{S}$  and create a controller with nominal input  $\bar{u}$  such that

$$\lim_{t \rightarrow \infty} \bar{e}(t) = \lim_{t \rightarrow \infty} (\bar{y}(t) - y_{\text{ref}}(t)) = 0. \quad (12)$$

- 2) Create a controller for the real system that guarantees

$$\lim_{t \rightarrow \infty} \underline{e}(t) = \lim_{t \rightarrow \infty} (y(t) - \bar{y}(t)) = 0. \quad (13)$$

where  $y_{\text{ref}}$  is the desired outlet temperature trajectory. The inner loop Lyapunov controller stabilizes the nominal tracking error, while the outer loop error stabilizer ensures convergence of the real system towards the nominal system. Combination of both systems ensures asymptotic convergence of the real system output towards the reference. As this convergence is not bound to parameters of the real system, robustness in presence of parametrical uncertainties is granted by design.

### C. Inner loop Lyapunov controller

Based on (12), a Lyapunov candidate  $V = \frac{1}{2} \bar{e}^T \bar{e}$  can be defined. With  $\dot{\bar{e}} = C[A\bar{\xi} + \bar{B}] - \dot{y}_{\text{ref}}$ , it follows that

$$\dot{V} = \dot{\bar{e}} \bar{e} = [C[A\bar{\xi} + \bar{B}] - \dot{y}_{\text{ref}}] \bar{e}. \quad (14)$$

Introducing  $\bar{K} \in \mathbb{R}^+$  allows to guarantee stability using the following equation forcing the derivative to be negative

$$\dot{V} = \dot{\bar{e}} \bar{e} = [C[A\bar{\xi} \bar{u} + \bar{B}] - \dot{y}_{\text{ref}}] \bar{e} = -\bar{K} \bar{e}^T \bar{e} < 0. \quad (15)$$

Solving for  $\bar{u}$  leads to a control law for the nominal plant model

$$\bar{u}(t) = \frac{-\bar{K} \bar{e}(t) - C\bar{B} + \dot{y}_{\text{ref}}}{CA\bar{\xi}(t)}, \quad (16)$$

which guarantees asymptotic convergence of the nominal system output towards the reference.

### D. Outer loop Lyapunov controller

Applying the same method to the error  $\underline{e} = y(t) - \bar{y}(t)$  leads to the equation

$$\dot{\bar{y}}(t) - \dot{y}(t) + \underline{K} [\bar{y}(t) - y(t)] = 0. \quad (17)$$

In order to introduce the system input  $u$  to the equation, a phenomenological consideration of the system output is used. The relative degree of the system being one allows

to represent the derivative of the system output as in the following equation:

$$\dot{y}(t) = F(t) + \alpha u(t) \quad , \quad (18)$$

with  $F(t)$  continuously updated according to

$$F(t) = \hat{y}(t) - \alpha u(t - \tau_w). \quad (19)$$

with  $\hat{y}$  obtained using any derivative estimation method for noisy data and  $\tau_w$  being the measurement window used for the estimation. Using  $\bar{K} = \underline{K} = K$  for simplicity, this representation leads to the control law

$$u(t) = \frac{1}{\alpha} \left( -F(t) + \dot{y}_{\text{ref}} + K(y_{\text{ref}} - y) \right) \quad , \quad (20)$$

with the constant  $\alpha = CA\xi|_{\xi_0}$  calculated for a reference state  $\xi_0$ . In defining  $\alpha$  for a reference, the need for an observer for the states  $\xi$  is eliminated, which can be interesting for practical use. In this work, the advantages of choosing  $\alpha$  dynamically, replacing the model reduction to allow for improved observer performance and expanding the model onto the pipe walls are investigated. This takes the theoretical approach [10] one step closer to a real world implementation, even though more aspects will need to be considered.

## IV. MODEL REDUCTION

The model reduction used in [9] and [10] is only used for calculation of the factor  $\alpha(t)$ , which is assumed to be constant in [10]. This work proposes a dynamic consideration of the nonlinearity described by  $\alpha$ . For this cause it is important to minimize the error between the states of the reduced order model and the true system states. The radial basis functions used in [9] and [10] are independent of the physical description of the solar plant. Hence, the use of simulation data, which are easily available using for example finite-differences or more elaborate methods, can improve the choice of the basis functions. This is the case for the proper orthogonal decomposition (POD) method, which can be used to create physically motivated basis functions and has been applied to thermal systems successfully as, e.g., in [12].

### A. Proper Orthogonal Decomposition

The POD works as follows: Given a typical solution of the PDE  $y(t, x)$  with  $t \in [0, t_{\text{end}}]$  and  $y(\cdot, x) \in \mathcal{H}$  for a suitable Hilbert space  $\mathcal{H}$  with inner product  $\langle \cdot, \cdot \rangle$ . The POD determines the (orthogonal) basis functions  $\gamma_j(x) \in \mathcal{H}$  by maximizing the projection of  $y$  onto the  $\gamma_j(x)$ , which yields

$$\max_{\tilde{\gamma}_1, \dots, \tilde{\gamma}_d} \int_0^{t_{\text{end}}} \sum_{j=1}^d \langle y(x, t), \tilde{\gamma}_j \rangle^2 dt, \quad s.t. \langle \tilde{\gamma}_i, \tilde{\gamma}_j \rangle = \delta_{i,j} \quad ,$$

with  $\delta_{i,j}$  being the Kronecker Delta. The solution to this optimization problem can be found in, e.g., [13]. For a set of discrete simulation data consisting of spatially discrete snapshots  $y_i = y(t_i, x) \in \mathbb{R}^{N_x}$  representing the discrete temperature distribution at time steps  $t_i$ ,  $i = 1 \dots N_t$  the procedure can be applied as follows [13]:

- 1) Construct  $Y = [y_1, \dots, y_{N_t}] \in \mathbb{R}^{N_x \times N_t}$ .
- 2) Calculate correlation matrix  $\mathcal{R} = YY^T \in \mathbb{R}^{N_x \times N_x}$ .

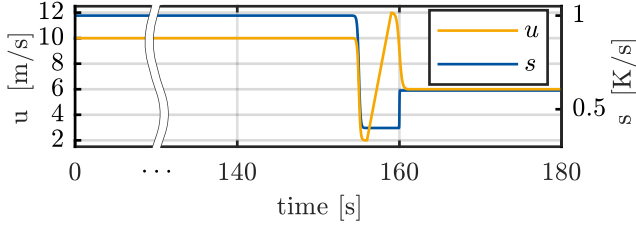


Fig. 2. Simulation input for creation of POD modes

- 3) Obtain Eigenvalues and eigenvectors from an Eigenvalue decomposition of  $\mathcal{R}$ :  $[\gamma, \Lambda] = \text{eig}(\mathcal{R})$ .
- 4) POD basis functions  $\{\gamma\}_{i=1}^d = \gamma_{\cdot, i} \in \mathbb{R}^{\mathcal{N}_x}$  and respective Eigenvalues  $\lambda_i = \Lambda_{ii}$ ,  $i = 1, \dots, d$ .

### B. Application to the solar collector

The snapshot-data  $Y$  is obtained using simulation data generated by a finite difference simulation of (2) with characteristic input and disturbance trajectories. As  $T_1(t)$  is assumed to undergo only slight changes during operation of the solar plant, its value is fixed at  $180^\circ\text{C}$ , while  $s$  and  $u$  follow the trajectories given in Fig. 2 with spatially constant  $s(x, t)$ . Using the simulation data directly as snapshot data set  $Y$  leads to bad results. This is caused by two effects: First, long stationary periods will force the quadratic cost function in (21) to solely focus onto the stationary behavior and not onto the dynamics. Second, the POD method will only reconstruct the boundary conditions accurately if they are homogeneous [12]. The first point is addressed by carefully selecting non-equidistant time steps  $t_i$  with

$$\begin{aligned} t_1 &= 0, \\ t_i &= \arg \min |t_i|, \\ &\text{s.t. } \max_x |y(t_{i-1}, x) - y(t_i, x)| \geq 0.005 \text{ K and } t_i \geq t_{i-1}. \end{aligned} \quad (21)$$

The second problem is solved by an adjustment which at the same time removes the mean value from the snapshot data known as centering trajectory approach. Therefore, the modified data set  $\tilde{Y}$  with  $\tilde{y}_i$  defined by

$$\tilde{y}_i = \frac{1}{y_i(0)} \left( y_i - \frac{1}{\mathcal{N}_t} \sum_{j=1}^{\mathcal{N}_t} y(t_j, \cdot) \right). \quad (22)$$

is used. Here, the term  $y_i(0)$  scales the snapshots using the left boundary value, whereas the time average is subtracted in the sum-term. This procedure results in a dataset, which contains homogeneous snapshots as  $T_1$  is kept constant. The choice of  $u$  and  $s$  ensure, that the running in behavior of the plant and reaction towards disturbances and setpoint changes are included as well. Applying the algorithm above to this dataset leads to the basis functions displayed in Fig. 3. For better comparison with the approximate model from [9], the basis functions from [9] (radial Gaussian functions) are depicted above. One can clearly observe, that the basis functions generated via POD show typical shapes of physical modes, which indicates a better physical representation of the process within the reduced order model.

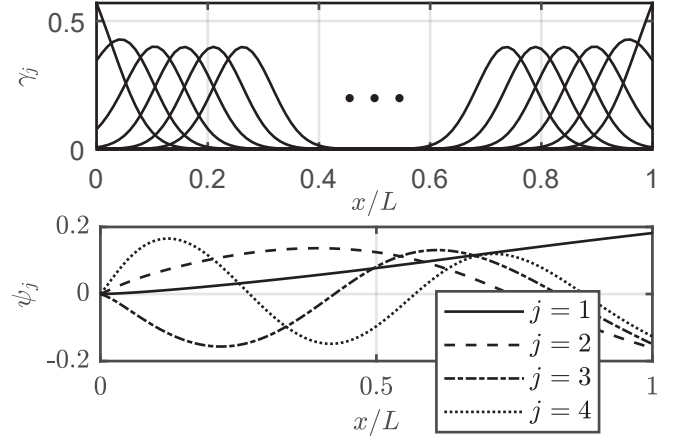


Fig. 3. Modes of the radial Gaussian approach (top) and the proper orthogonal decomposition approach (bottom)

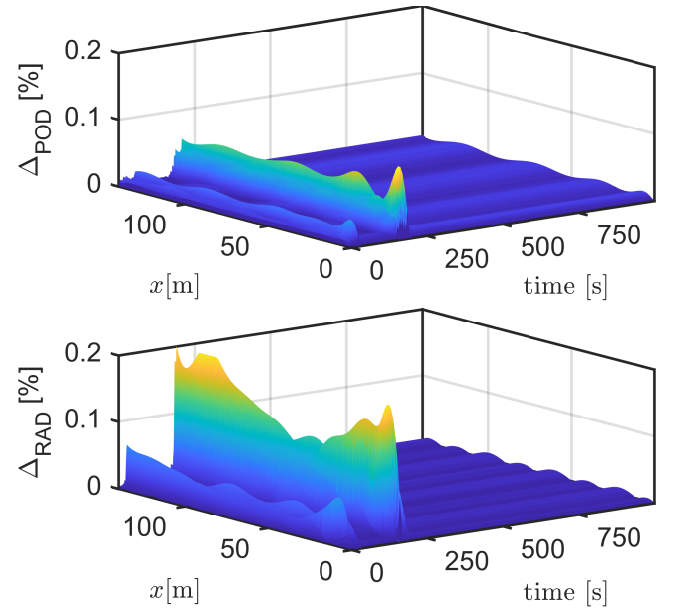


Fig. 4. Simulation results of model reduction methods with  $d = 8$  modes

### C. Verification of the model reduction

The reduced order model is now validated using two different methods: First, results of a simulation of the plant behavior using the POD modes is compared to a high dimensional finite difference simulation of the plant and to the approximate model from section III. Second, the system behavior in the frequency domain is analysed concerning the anti-resonance modes first presented in [14]. A comparison of the exactness of the model reduction procedures concerning highly resolved simulations is displayed in Fig. 4. Thereby, the relative error

$$\Delta(x, t) = \left| \frac{\hat{T}(x, t) - T_{\text{real}}(x, t)}{\text{mean}_{x,t}(T_{\text{real}}(x, t))} \right|. \quad (23)$$

is depicted. Note that for both (radial basis functions and POD) eight basis functions are used as in [9]. Further note

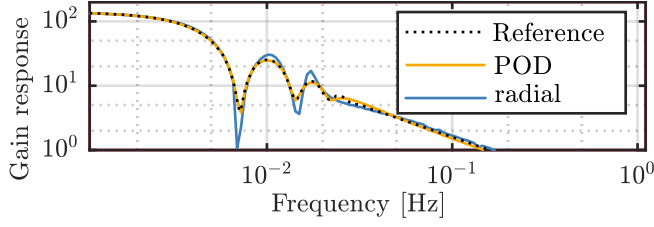


Fig. 5. Gain response for model reductions and reference at  $u = 1 \text{ m s}^{-1}$

that the simulation data used to derive Fig. 4 significantly differed from the snapshot data by choosing different functions for  $u(t)$  and  $s(t)$ .

The comparison of both sets of basis functions shows low errors for stationary behavior of the plant for  $t > 250 \text{ s}$  for both of them. But especially for sequences of big changes in input and disturbance terms the model reduction using radial basis functions creates larger errors and overall worse performance than the POD model. Even though the performance level is good ( $\Delta < 0.2\%$ ), a smaller error - as indicated from the POD - will allow higher controller gains  $K$  and improved performance of observers, as the difference  $y - y_{\text{ref}}$  will be met more exactly.

Another comparison of interest is the systems gain response. Again, simulations using the POD method and radial basis functions are compared to a high dimensional finite difference simulation of the system. The gain response plots shown in Fig. 5 are obtained applying harmonic oscillations of the sun intensity to the system at constant fluid velocity. For further detail on the procedure, refer to [14]. The frequency of the expected anti-resonance modes is correct for both model reductions. The model reduction using radial basis functions overestimates those modes, while the POD model reduction properly catches the first three anti-resonance modes. The comparison of the model reduction procedures show that the POD model reduction yields better results for relevant model properties and is thus used to replace the Gaussian model reduction. This replacement promises higher controller gains and also improved performance in observers and calculation of process values.

## V. EXTENSION OF THE CONTROLLER

The controller presented in section III is based on the simplified model of the plant (2). As the model in (2) does not contain the temperature of the surrounding metal pipe, it has to be assumed, that  $T = \vartheta$  holds when applying this controller. This assumption will not be fulfilled in a physical plant and thus limits the applicability of the controller. In the following we will relax this assumption by extending the controller scheme from (2) to (5) along with incorporating the model reduction and a third improvement.

### A. Application of the model reduction

Beginning with (5) the model reduction can again be applied to the oil and wall temperatures,

i.e.  $\hat{T} = \Gamma\xi$ ,  $\hat{\vartheta} = \Gamma\zeta$ , leading to

$$\dot{\xi}(t) = u(t)A\xi(t) + A'(\xi(t) - \zeta(t)) \quad (24)$$

$$\dot{\zeta}(t) = A''(\xi(t) - \zeta(t)) + B'(t) \quad (25)$$

$$y(t) = C\xi(t) \quad (26)$$

with respective initial and boundary conditions as before.  $A' = -\hat{\lambda}I_{d \times 1}$ ,  $A'' = \hat{\lambda}I_{d \times 1}$  and  $B'(t) = (\Gamma^T\Gamma)^{-1}\Gamma^T\hat{p}(t)$ . For a constant disturbance  $\hat{p}(x, t) = \hat{p}$ , a nominal system can be defined analogously to Section III:

$$\dot{\bar{\xi}}(t) = \bar{u}(t)A\bar{\xi}(t) + A'(\bar{\xi}(t) - \bar{\zeta}(t)) \quad (27)$$

$$\dot{\bar{\zeta}}(t) = A''(\bar{\xi}(t) - \bar{\zeta}(t)) + \bar{B}'(t) \quad (28)$$

with  $\bar{B}'(t) = (\Gamma^T\Gamma)^{-1}\Gamma^T\hat{p}$ .

### B. Inner loop Lyapunov control

Using the same procedure as in section III, a nominal error  $\bar{e}(t) = \bar{y}(t) - y_{\text{ref}}(t)$  is defined and its derivative represented by  $\dot{\bar{e}}(t) = C\bar{u}(t)A\bar{\xi}(t) + CA'(\bar{\xi}(t) - \bar{\zeta}(t)) - \dot{y}_{\text{ref}}(t)$ . Again, the Lyapunov function  $\bar{V} = \frac{1}{2}\bar{e}^T\bar{e}$  is set up, which yields

$$\dot{\bar{V}} = \dot{\bar{e}}\bar{e} \quad (29)$$

$$= [C[\bar{u}A\bar{\xi} + A'(\bar{\xi} - \bar{\zeta})] - \dot{y}_{\text{ref}}]e \quad (30)$$

To achieve stability of the nominal tracking error, negative definiteness of  $\dot{\bar{V}}$  is enforced using  $\bar{K} \in \mathbb{R}^+$

$$[C[\bar{u}A\bar{\xi} + A'(\bar{\xi} - \bar{\zeta})] - \dot{y}_{\text{ref}}]e = -\bar{K}\bar{e}^T e \quad (31)$$

$$\Leftrightarrow \bar{u}(t) = \frac{-\bar{K}\bar{e} + CA'(\bar{\zeta}(t) - \bar{\xi}(t)) + \dot{y}_{\text{ref}}}{CA\bar{\xi}(t)} \quad (32)$$

The primary difference to the nominal control law in (16) is in the formerly unknown disturbance term, which has been replaced by the difference between the oil and pipe wall states. Thus, the extended controller uses more knowledge about the process to control.

### C. Outer loop error stabilizer

To reach tracking for the real model the same procedure is applied to the difference between real system output and nominal system output  $e(t) = \bar{y}(t) - y(t)$ . Using the Lyapunov candidate  $V(t) = \frac{1}{2}e^T e$  and forcing  $\dot{V} = -\underline{K}e^T e$  with  $\underline{K} = \bar{K} = K$ , leads to the necessary condition for stability of the tracking error:

$$\dot{\bar{y}}(t) - \dot{y}(t) + K[\bar{y}(t) - y(t)] = 0 \quad (33)$$

As neither the nonlinear term nor the system output have changed, the relative degree of the system is still one. This allows to represent the derivative of the system output as

$$\dot{y}(t) = F(t) + \alpha(t)u(t) + \beta(t) \quad (34)$$

with  $\alpha(t) = CA\xi(t)$  and  $\beta(t) = CA'(\xi(t) - \zeta(t))$ . This leads to the final control law

$$u(t) = \frac{1}{\alpha(t)} \left( -F(t) + \dot{y}_{\text{ref}}(t) + K[y_{\text{ref}}(t) - y(t)] \right), \quad (35)$$

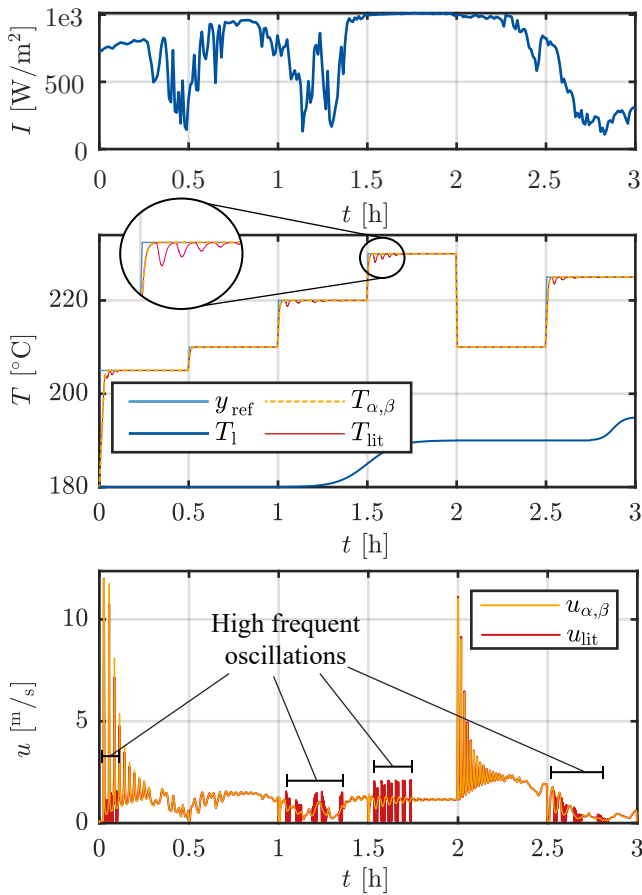


Fig. 6. Simulation input data for validation:  $I$  is the solar irradiance profile,  $T_1$  describes the left boundary condition,  $T_{\alpha,\beta}$  is the improved controller,  $T_{lit}$  the literature controller and  $u$  the input trajectories respectively.

with  $F(t)$  continuously updated according to  $F(t) = \hat{y}(t) - \alpha(t)u(t - \tau) - \beta(t)$ . As opposed to the representation in section III, the parameters  $\alpha$  and  $\beta$  are not created for a given setpoint and then set to a constant value but calculated dynamically. This dynamic calculation requires knowledge of the system states, which can e.g. be gained using an observer. Using the improved model reduction presented in section IV greatly improves the accuracy of these observers, as the overall model accuracy is increased. As the parameter  $\alpha$  is inverted during calculation of the control law,  $\alpha$  is bounded below  $-0.1$  to prevent  $\alpha = 0$ .

## VI. CONTROLLER RESULTS

For validation of the proposed control law, several simulations have been conducted using the simulation procedure described in [2] without consideration of heat losses to the environment. The test scenario in Fig. 6 is taken from sun intensity measurements in [2]. In [10] results for  $K = 0.005$  have been shown. For this very low controller gain the difference between the former and the extended Lyapunov controller are quite small as the system response is slow and the improvements do not affect the result that much. For an increased  $K = 0.05$  (refer to Fig. 6), the reference controller from the literature tends to create high frequent oscillations

in the system input and also shows oscillations in the system output  $T$ . Using the enhanced controller, the oscillations in  $T$  are cancelled out and a smooth first-order behavior can be observed. Also in  $u$  an improvement can be seen: Even though the amplitude of the changes in  $u$  is increased, the frequency of  $u$  is much smaller. Hence, by introducing more system knowledge, the available tuning range of parameters has been improved significantly allowing for more aggressive controller settings which reduce settling time.

## VII. CONCLUSION

The bilinear Lyapunov controller from literature has been improved in this paper in regard of three aspects: A novel model reduction has been presented, which shows increased precision. Further, the extension of the control structure with the pipe temperature and the choice of variable  $\alpha$  along the improved model reduction allows for a drastically more aggressive tuning of the controller without taking the risk of oscillations. Ongoing work will deal with the design of the necessary observers and a comparison of enhanced Lyapunov controller with distributed control strategies.

## REFERENCES

- [1] A. McCrone, U. Moslener, F. d'Estais, and C. Grüning, "Global trends in renewable energy investment report 2018," 2018.
- [2] E. F. Camacho, M. Berenguel, and F. R. Rubio, *Advanced Control of Solar Plants*, ser. Advances in Industrial Control. London: Springer, 1997.
- [3] E. F. Camacho, M. Berenguel, and A. J. Gallego, "Control of thermal solar energy plants," *Journal of Process Control*, vol. 24, no. 2, pp. 332–340, 2014.
- [4] F. O. R. Vaz and R. Neves da Silva, "PID control of a solar plant with gain interpolation," in *Proceedings of the 2nd Users Workshop Training and Mobility of Researchers Programme at Plataforma Solar de Almería*, ser. Serie ponencias. Madrid: Ed. CIEMAT, 1998.
- [5] D. Limon, I. Alvarado, T. Alamo, M. Ruiz, and E. F. Camacho, "Robust control of the distributed solar collector field acurex using mpc for tracking," *IFAC Proceedings Volumes*, vol. 41, no. 2, pp. 958–963, 2008.
- [6] P. Gil, J. Henriques, P. Carvalho, H. Duarte-Ramos, and A. Dourado, "Adaptive neural model-based predictive control of a solar power plant," in *Proceedings of the 2002 International Joint Conference on Neural Networks*. Piscataway, N.J: IEEE, 2002, pp. 2098–2103.
- [7] C. M. Cirre, M. Berenguel, L. Valenzuela, and E. F. Camacho, "Feedback linearization control for a distributed solar collector field," *Control Engineering Practice*, vol. 15, no. 12, pp. 1533–1544, 2007.
- [8] C. M. Cirre, J. C. Moreno, M. Berenguel, and J. L. Guzmán, "Robust control of solar plants with distributed collectors," *IFAC Proceedings Volumes*, vol. 43, no. 5, pp. 823–828, 2010.
- [9] S. Elmetennani and T.-M. Laleg-Kirati, "Bilinear reduced order approximate model of parabolic distributed solar collectors," *Solar Energy*, vol. 131, 2016.
- [10] S. Elmetennani and T. M. Laleg-Kirati, "Bilinear approximate model-based robust lyapunov control for parabolic distributed collectors," *IEEE Transactions on Control Systems Technology*, vol. 25, no. 5, pp. 1848–1855, 2017.
- [11] W. Platzer and C. Hildebrandt, "Absorber materials for solar thermal receivers in concentrating solar power (CSP) systems," in *Concentrating solar power technology*, ser. Woodhead Publishing series in energy, K. Lovegrove and W. Stein, Eds. Oxford and Philadelphia: Woodhead Publishing, 2012, pp. 469–494.
- [12] L. Pyta, F. Nolteernsting, and D. Abel, "Verteilparametrische Modellierung und Regelung eines thermischen Festbetspeichers," *at - Automatisierungstechnik*, vol. 65, no. 5, 2017.
- [13] S. Volkwein, *Proper Orthogonal Decomposition: Theory and Reduced-Order Modelling*, 2013.
- [14] A. Meaburn and F. M. Hughes, "Resonance characteristics of distributed solar collector fields," *Solar Energy*, vol. 51, no. 3, pp. 215–221, 1993.